Constrained Positron Flight in PET Imaging via Strong Magnetic Fields

A Senior Honors Thesis

Presented in partial fulfillment of the requirements for graduation *with research distinction* in Physics in the undergraduate colleges of the Ohio State University

by

David Albani

The Ohio State University
June 2008

Project Advisor: Professor Klaus Honscheid, Department of Physics

Abstract - Positron Emission Tomography (PET) imaging is a noninvasive imaging technique that utilizes radioactive emissions to produce positron-electron annihilations. Annihilation events result in the production of a pair of detectable photons that travel anti-parallel to one another with a slight angle of acollinearity. PET imaging has found use in the field of medicine by attaching radiotracers to materials such as sugars and antibodies, where metabolizing these agents allows for the observation of specific internal regions of the patient. Dependent on the region to be observed, radioisotopes of varying energy spectra are attached to the appropriate agent and introduced to the patient. Higher-energy isotopes emit positrons that tend to travel further prior to annihilation, which correlates to poorer image resolution. This is because a higher-energy positron must scatter off of more electrons than a lower-energy positron in order to lose enough energy that an annihilation event is likely. Poor image resolution is also associated with imaging in less dense media, as the positron must travel further on average in order to collide with an electron. As the positron, the anti-particle of the electron, possesses the property of charge, the presence of a strong magnetic field can constrain the flight of the positron to a helical path. By constraining the flight of the positron, the average distance from the source to the annihilation point is reduced. While the positron travels the same distance overall, the displacement of the positron from its source is reduced, resulting in images with better resolution. Simulations of the imaging process in the absence and presence of strong, homogeneous magnetic fields have shown the theoretical effectiveness of performing PET scans in the presence of a strong magnetic field. In collaboration with the Ohio State University Medical Center, the laboratory of Dr. Klaus Honscheid has tested a novel silicon-silicon small-animal PET system in the presence of a 7 Tesla magnetic field. The experimental data agrees well with the predictions made by simulation.

I. Introduction

Radioactive elements contain a very important property: the process of decay. Decay transforms an isotope of a particular form, the parent nuclide, into a different form, known as the daughter nuclide. Nuclear decay involves three types of transformations of particular interest: alpha, beta, and gamma decay. The emission of a positively-charged nucleus containing two protons and two neutrons is known as alpha decay, while the release of a high-energy (greater than about 10 keV) photon is referred to as gamma radiation. Beta radiation takes on two forms, beta-negative and beta-positive decay, where beta-negative decay releases an electron and beta-positive decay emits a positron, the positively charged anti-particle of the electron. In each of these instances, the release of a particle corresponds to a loss of energy and a transformation to a more stable state for the parent atom [1].

Radioactive phenomena have been applied to a number of fields, and these properties were first applied to medical imaging through X-ray radioagraphy. X-ray photons were used to create visible images from non-visible radiation for the first time in 1895 [2], providing structural information about a patient. Since that time, more sophisticated techniques of non-invasive imaging have been developed, providing information about metabolic and other functional features of a patient in addition to structural images. Of particular note is the advent of tomographic imaging techniques, where two-dimensional slices and three-dimensional volume images are compiled from projection images obtained over a series of planes. Pixels (2D) and

voxels (3D) in tomographic images represent small areas or volumes in space where a measurable parameter is detected. Planar imaging methods, employed prior to the onset of tomography, integrate information about the measurable parameter over a volume of space and project the distribution onto a plane [3].

With the development of sophisticated algorithms to perform image reconstruction, tomographic techniques began playing an important role in medical diagnosis and research imaging. The combination of tomographic imaging methods with radiation detection systems has led to a number of medical imaging techniques that are employed today. Amongst these techniques are Single Photon Emission Computed Tomography (SPECT), X-ray Computed Tomography (CT), and Positron Emission Tomography (PET) [2]. PET imaging, in which positrons released by a radioactive isotope are used to observe processes within a patient, is the focus of this study.

PET imaging is accomplished through the use of a positron-emitting radioactive isotope, a photon detector, a data acquisition device, and a computer to reconstruct the image from the data. The radioactive tracer used in a scan will collect in specific regions of the host, where large amounts of tracer in a region correspond to an image with bright spots that stand out against a relatively dark background, where little of the tracer has collected. A commonly used radiotracer for PET scans is F^{18} fluoroudeoxy-D-glucose (F-FDG). This tracer is particularly useful in brain scans for its ability to highlight regions of neural activity, and it has also found use in cancer imaging, as the increased metabolism of malignant tumor cells allows much of the tracer to collect in the cancer cells and greatly stand out in contrast to healthy body cells [4]. The region to be imaged dictates the type of tracer to be used in a scan; some atoms attach more strongly than others to the sugars, antibodies, and other carriers used to introduce the isotope to the body, thus the type of carrier used limits what type of isotopes can be used for imaging. This fact has implications that shall be explored later.

The photon detection system in traditional PET systems utilizes a scintillating crystal to detect photons. The crystals scintillate, or emit light, in response to the ionizing photon radiation, where the light pulses emitted by the scintillator pass through photomultiplier (PM) tubes or avalanche photodiodes (APD) [1]. These pulses are passed from the PM or APD system to an analog-to-digital converter (ADC) and converted to an electrical signal that is then transferred to a computer for processing. Once a complete data set is obtained, a mathematical algorithm is applied to the information to produce a reconstruction of the source environment. Every aspect of this sophisticated technology has the potential for improvement; using different carriers to embed the radiotracer, changing the scintillating crystals, or applying additional algorithms can improve the resolution of PET imaging systems.

Positron emission tomography provides an important tool in both medical diagnoses and research settings. Depending on the agent transporting the radioactive isotope, a variety of body regions can be imaged by PET. In particular, these images reveal processes such as metabolism and the distribution of pharmaceuticals. Following metabolism is important in a research setting, as it helps in developing a better understanding of body functions. In a medical imaging setting, its value is seen through distinguishing highly metabolic cancer cells within the body. As organs and the structures that surround them within the body are highly complex, it serves the interest of

the imaging community to achieve the best resolution possible when scanning. Small animals are typically used in the context of pharmaceutical research and disease progression studies, hence the development of dedicated small-animal PET scanners. The best small-animal research scanners today have image resolution on the order of ~2 mm, while human scanners have resolution on the order of 6-10 mm [5].

To achieve optimal image resolutions, we have investigated the advantages and challenges of a silicon-silicon pad detector system. The use of semiconducting silicon detectors differs from traditional PET detection systems in a few important ways. Primarily, the silicon pads are produced at a much smaller size than traditional scintillating crystal systems. A detector system consists of an array of these silicon pads in a much denser configuration than traditional scintillators allow for. Additionally, detection of photons in the silicon chips occurs through Compton scattering of photons off of electrons, rather than scintillation. Testing of this novel system has revealed a substantial increase in resolution over traditional detection methods corresponding to the small pad size and has also brought new resolution limitations to light [6].

II. The PET Imaging Process

The process of PET imaging initiates with a beta decay from a radioactive isotope that results in the emission of a positron. In a medical imaging setting, the positron has an energy that ranges from a few hundred keV to a few MeV. Since radioactive beta-positive decay is a three-body process with the release of a positron, neutron, and neutrino, the initial energy of the positron varies from zero to a maximum value that is characteristic of its emitting isotope. Following emission, the positron travels until it collides with and scatters off of electrons in the surrounding environment, its energy decreasing with each interaction. An annihilation event is most likely to occur as the positron approaches zero kinetic energy, which can also be defined as 511 keV total energy, the rest mass of both the positron and electron. At this point, interaction with an electron will result in the creation of a positronium, a very unstable electron-positron system that decays via annihilation [7].

Positron-electron annihilation is an event that produces a pair of photons traveling anti-parallel to one another, each at an energy of 511 keV. Per conservation of momentum, the photons travel with a slight angle of skew, known as acollinearity, when the total momentum of the positron-electron system is slightly greater than zero as the particles annihilate [8]. The photons are energetic enough to pass through host tissues with a very small likelihood of scattering, as the cross-section for 511 keV photons to interact in the body is small. Outside of the patient, the photon will be detected by position-sensitive photodetectors. In traditional systems, scintillating materials absorb the ionizing photons, which produces light that is converted to a signal above typical noise levels through either a PM or ADP system. The spatial orientation and timing of these impulses are transmitted to a computer for later analysis.

For clinical PET systems, signals from opposite detector regions that occur within 6-12 ns of each other can be considered simultaneous events, or photons in coincidence, meaning that the photons triggering the signals likely came from the same annihilation event. Drawing a line between the coincident photon detection points indicates a line along which the point of the

positron-electron annihilation occurred, referred to as a line of response (LOR). When a sufficient number of events are sampled, a reconstruction algorithm is applied, which incorporates all of the lines drawn between coincidence points and constructs an image that resembles the emitting isotope region. An important component of the reconstruction process is the sinogram, a diagram that incorporates each LOR by drawing the shortest line connecting a central point to the LOR. The sinogram represents the radial components of these lines drawn to each LOR, where the radius and angle of each line drawn to an LOR is represented as a pixel on the sinogram [9].

III. Limitations on Scanning Resolution

In collaboration with the University of Michigan, the laboratories of Drs. Klaus Honscheid and Harris Kagan at the Ohio State University have developed a novel PET scanner. The detector system consists of two silicon detectors, each containing an array of 512 pads and measuring 1.4 mm x 1.4 mm x 1 mm thick, arranged in a 32 x 16 configuration. Conventional PET scanners often incorporate a ring of detectors that fully surround the patient. As both materials cost and manufacturing considerations made it more practical to incorporate only two detectors into the system, it was necessary to simulate a ring of detectors. To emulate the effect of having a ring of detectors, the prototype system incorporates a turntable that can be rotated by a pneumatic pump in one-degree increments. This rotation of the source allows emission data to be collected from all sides of the source, as it would be in a ring of detectors. The completed detector prototype is shown in Figure 1, where the system has been tested in the presence and absence of magnetic fields. Testing of the system under optimal conditions determined a resolving power of 0.7 mm FWHM [6]. At these high resolutions, it has been found that the flight distance of the positron prior to annihilation is the ultimate limitation on resolution.

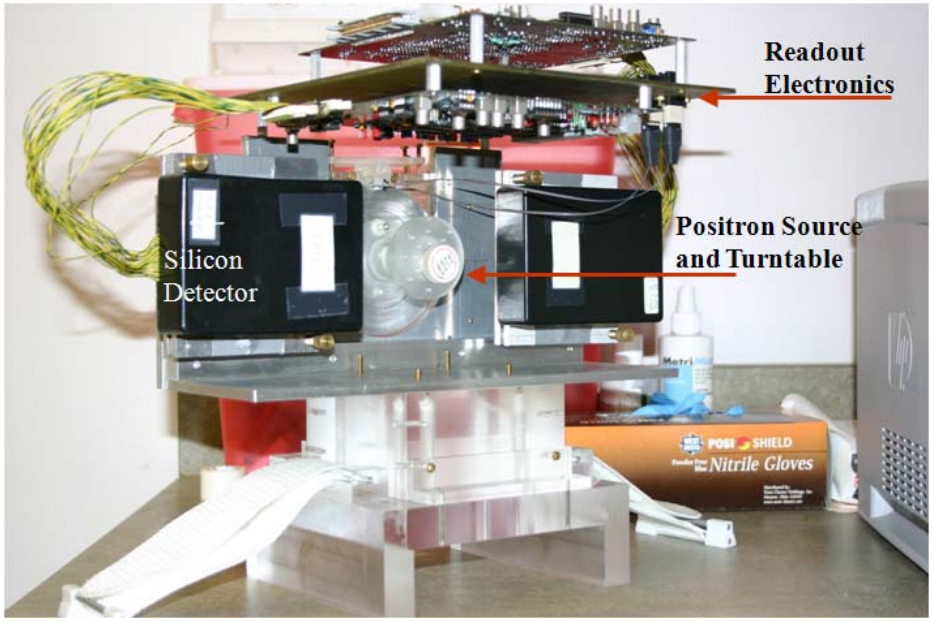

Figure 1: The silicon-silicon detector system composed of non-magnetic elements. Photo courtesy Don Burdette.

Two elements can be attributed to the travel distance of the positron: initial energy and environment. Particularly, there are low-energy and high-energy isotopes that have been synthesized for use in PET scans, where the resolution of the final image degrades as the energy of the emitted positron increases. The electron-density of the environment in which the positron is released also plays a significant role in determining image resolution. The body is composed largely of water, and consequently most of the internal organs of an organic host display characteristics similar to this electron-dense medium. Conversely, images of structures such as the lungs, which have roughly a third of the density of typical organs, have poorer resolution. The degradation in resolving power for both higher energy isotopes and low density media directly corresponds to the fact that positrons in these situations must travel further prior to annihilation.

The positron is a charged particle with the same magnitude of charge and opposite polarity of the electron. Given these traits, the positron is able to be manipulated by magnetic fields. In the absence of a magnetic field, a beta positive decay source will emit positrons in a spherically symmetric distribution. Magnetic forces act perpendicular to the direction of the magnetic field, therefore the flight of a positron will be unaffected only if it is travelling parallel to the magnetic field. As positrons are emitted in all directions with equal likelihood and scatter multiple times off of electrons, the trajectory of almost every positron will be affected by the magnetic field. Particularly, the velocity components of the positron in the direction perpendicular to the B field will change such that the positron curves around the magnetic field. It is proposed, therefore, that a strong magnetic field emitted in the direction transverse to the imaging plane will effectively constrain positron flight to a circular path in that plane, thereby reducing the total displacement of the positron while the net distance traveled remains the same [10]. This will reduce the displacement of annihilation events from the positron source, thus improving the resolving power of the detector system. Simulations have been performed to anticipate and verify the effects of static magnetic fields on the PET imaging process.

IV. Simulation of the PET Process

Simulation of the PET process has provided a means of testing our ideas from the basis of first physical principles and has guided the development of our prototype scanner. The primary software used to conduct the simulations is Electron Gamma Shower 4 (EGS4), developed and distributed by the Stanford Linear Accelerator Center (SLAC) [11]. This programming utility provides the user with environmental construction tools and the ability to define particles and emission conditions. A shower of particles is generated through this software, where particle movements and interactions are followed in iterative steps. Outside of this particle simulation software, C++ and ROOT were used to perform mathematical and graphical checks on the simulation. Once particle simulation was complete, Matlab was used to perform reconstruction algorithms on the data.

Simulation was initiated by generating an energy spectrum for each of the radioactive isotopes to be tested. In particular, an algorithm was chosen that incorporated the atomic number of the isotope to determine the energy distribution as shown here:

$$N(E)\mathrm{d}E = gF(Z,E)pE(E_{max} - E)^2\mathrm{d}E, \quad (1)$$

where $N(E)$ is the number of decays at energy E, g is a coupling constant, E is the total β energy in units of mc^2, E_{max} is the maximum (end point) energy of the β particle in units of mc^2, p is the momentum of β in units of mc, $F(Z, E)$ is the Fermi function, and Z is the atomic number of the beta decay daughter [12]. The Fermi function associated with this energy distribution took the Coulomb interaction between the beta and the daughter nucleus into account. A non-relativistic approximation for $F(Z, E)$, valid for *allowed* transitions of lighter elements had the form

$$F_{allowed}(Z, E) = 2\pi\eta/(1 - e^{-2\pi\eta}), \quad (2)$$

with $\eta = - Z\alpha E/p$ for positron decay, and $\alpha = 1/137$, the fine structure constant [12]. The distributions generated through this equation were analyzed graphically as shown in Figure 2 and compared to a theoretical energy distribution.

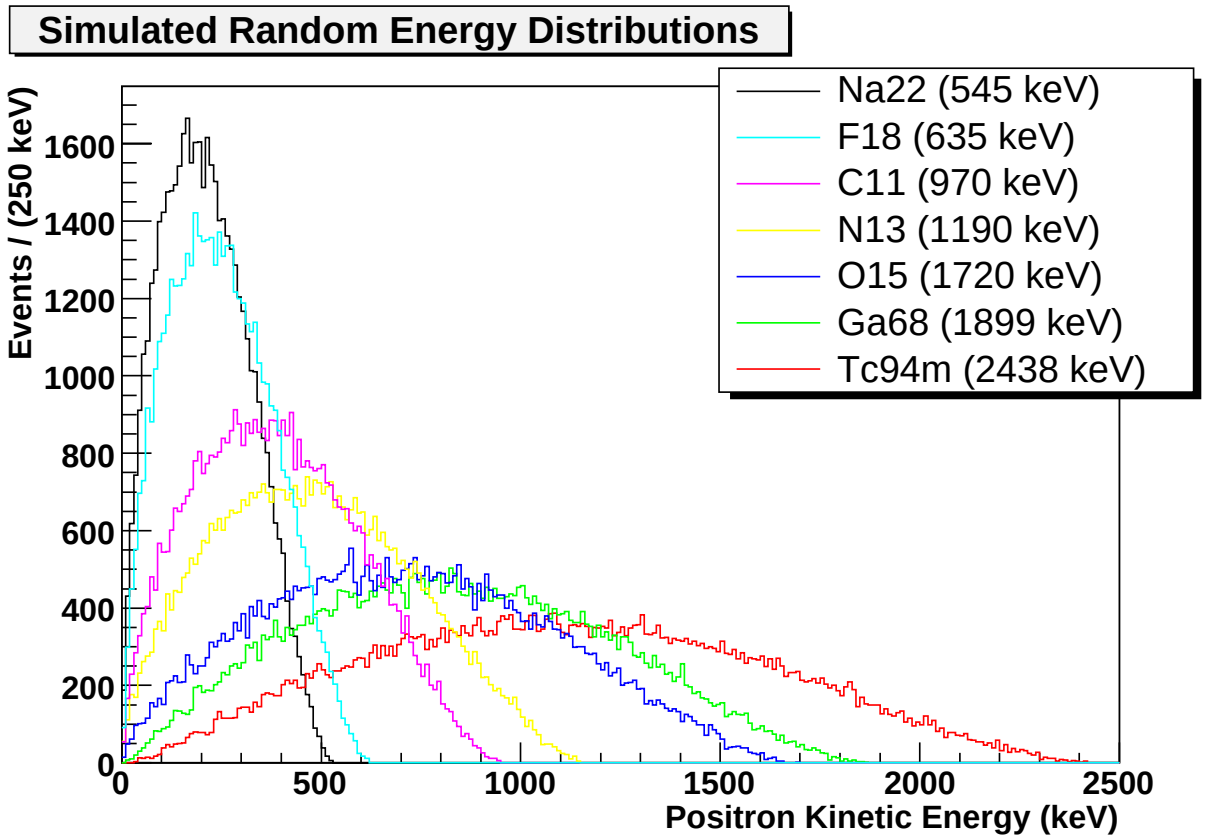

Figure 2: The distribution of energy levels at which positrons were emitted from the simulated source for various isotopes.

Once a random list of the allowed energies for a particular isotope was generated, EGS4 was utilized to perform the first step of the simulation - the emission of positrons in an environment. A pre-processor for EGS4, called PEGS4, was used to simulate the medium in which the particles were emitted. The cross-section data generated by PEGS4 was then called upon by the EGS4 program. A single event constituted the emission of a positron that then scattered off of electrons in the environment until an annihilation event occurred. A trial typically consisted of a few million of these events. Point sources that emitted positrons in all directions were initially used for testing until a disk source subroutine was implemented. Disk sources emitted positrons

with equal likelihood at any point along the disk. The position of positron annihilation was recorded and analyzed to verify an appropriate distribution of positrons around the source in the form of scatter plots and histograms as in Figure 3.

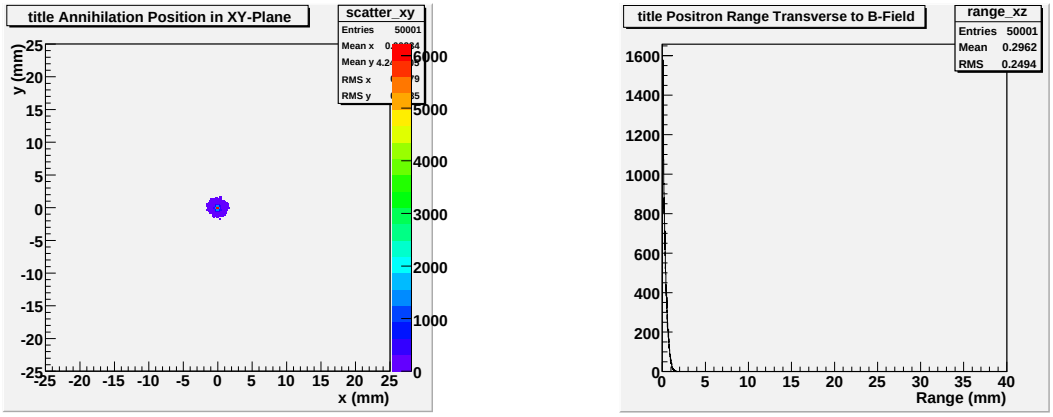

Figure 3: Positron annihilation positions in the XY-plane and the range of positron flight in the XZ-plane in the simulation of a ^{22}Na point source.

The environment of the positron emission trial was characterized by the medium in which the radioactive isotope was embedded as well as the magnitude and direction of the applied magnetic field. EGS4 was distributed without a routine for tracking particles in the presence of a magnetic field; consequently, a means of simulating the presence of a magnetic field was implemented. The static magnetic field was implemented via a subroutine from the SLAC documentation, entitled UCBEND, which imparted iterative curvature on the flight path of the positron [11]. The series of equations utilized to iteratively change the path of the particle was derived from general magnetic force equations, starting with

$$\vec{F}_{mag} = q(\vec{v} \times \vec{B}), \tag{3}$$

the general equation for the force experienced in the presence of a homogeneous magnetic field. Here, $\vec{F}_{mag}$ is the force asserted by the magnetic field, q is the charge the particle being affected by the magnetic field, $\vec{v}$ is the velocity of the particle traveling in the magnetic field, and $\vec{B}$ is the vector representing the magnetic field. Expanding the cross product into its Cartesian components and applying Newton's 2nd law of motion yields

$$\begin{aligned} ma_x &= q(v_y B_z - v_z B_y) \\ ma_y &= q(v_z B_x - v_x B_z), \\ ma_z &= q(v_x B_y - v_y B_x) \end{aligned} \tag{4}$$

where m is the mass of the particle, a_x (for example) represents the x-component of acceleration, v_x is the velocity component in the x-direction, and B_x represents the component of the magnetic field acting in the x-direction. On the basis of these equations, it can be observed that the magnetic force acts perpendicular to the magnetic field direction. Approximating the step length of the particle to be small, Δt, as it is in the context of an EGS4 simulation, and in the presence of a constant B field, a vector expression can be derived for the change in direction experienced by a particle in a magnetic field:

$$\hat{v} = \hat{B}(\hat{v}_0 \cdot \hat{B}) + [\hat{v}_0 - \hat{B}(\hat{v}_0 \cdot \hat{B})]\cos\alpha - \hat{v}_0 \times \hat{B}\sin\alpha, \quad (5)$$

where $\alpha = \Delta t/R$, R is the radius of curvature qp/B, where p is the particle momentum, $\hat{B}$ is the magnetic field unit vector, $\hat{v}_0 = U_0\hat{i} + V_0\hat{j} + W_0\hat{k}$ is the particle direction unit vector prior to magnetic influence, and $\hat{v} = U\hat{i} + V\hat{j} + W\hat{k}$, the particle direction unit vector after the particle experiences the magnetic force. Given that $\Delta t/R << 1$ and the magnetic field is emitted in the $\hat{j}$-direction, the equations describing the step-wise curvature imparted upon the particle would be

$$\begin{aligned} U &= (U_0 + \alpha W_0)F \\ V &= V_0 \qquad\qquad , \\ W &= (W_0 - \alpha U_0)F \end{aligned} \quad (6)$$

where $F=(1+\alpha^2)^{-1/2}$, the unit vector renormalization factor [11]. The effect of the simulated magnetic field was first tested by tracing every interaction of positrons in the absence and presence of a strong magnetic field, as shown in Figure 4.

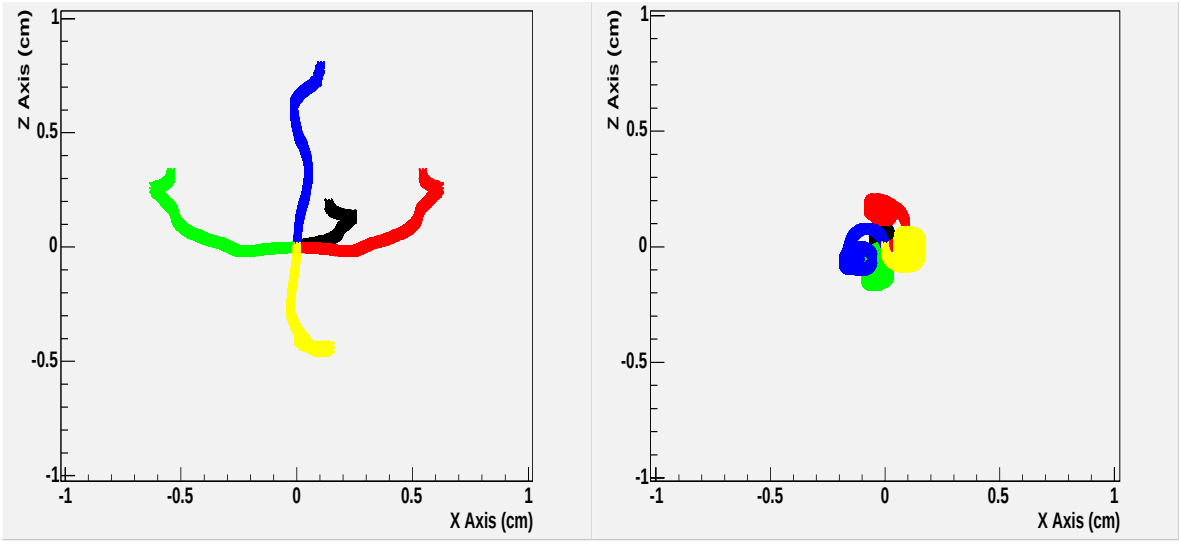

Figure 4: Observing each interaction of five separate positrons from the point of emission until annihilation. The left image shows the emission of positrons from a ^{94m}Tc source at the maximum energy of 2470 keV in an environment with no magnetic field. The right image shows the influence of a 9 Tesla magnetic on the same positrons, with the positrons confined to a cyclic path close to the point of emission in the plane transverse to the magnetic field.

Following emission of positrons, a C++ routine was run to generate a random series of acollinearity angles. The annihilation positions from the previous trial and the acollinearity angles were read in during a subsequent trial on EGS4. In this script, the positron annihilation position served as the emission point of a pair of photons. The photons travel almost entirely anti-parallel to one another, with a skew angle distribution of 0.54 FWHM degrees imparted as dictated by the read-in acollinearity value [8].

The simulated photon emission environment closely mimics the experimental set-up of the silicon detector system. The starting region for photon emission is schematically represented in Figure 5, where an air medium is flanked by two rectangles of silicon that are spaced 16.8 cm apart, as in the set-up of the prototype detectors. As annihilation events produce photon pairs, two photons would be emitted from a single positron annihilation point. Photons were confined to the imaging plane, for the sake of processing efficiency, and emitted in a random direction from the annihilation point. The interactions of the photon were followed as it traveled through the environment, where it either Compton scattered off of an electron in the silicon detector regions or passed through the detector plane entirely. After simulation of the first photon of the pair was concluded, the second photon would be emitted travelling anti-parallel to the first photon, where a small angle of acollinearity was incorporated to better match reality. To simulate the rotation of the radioisotope source on the turntable, the positron annihilation points in the simulation were rotated by an angular increment over a set interval of events.

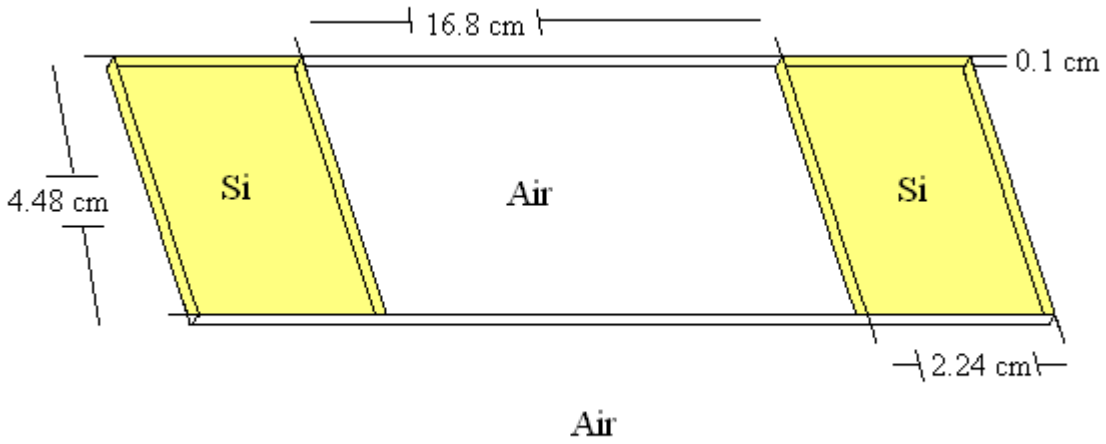

Figure 5: Schematic of the photon emission environment, where the two silicon regions represent the two photodetectors.

After the photon generation trial concluded, the output data was scanned for coincidence events. This was achieved through use of a C++ script that scanned through every interaction of each photon generated. Particularly, the script searched for photons originating from the same annihilation event that had each Compton scattered once off of electrons in opposite silicon detector regions. Under the simulation conditions, only ~20% of the events were viable.

Final image reconstruction began with the generation of a sinogram, as per typical PET image reconstruction techniques (Figure 6). Once a sinogram was constructed, the array was passed to a Matlab script for analysis. On the basis of detection points, lines of response are drawn between coincident photon detection events. Utilizing a maximum likelihood-expectation maximization (ML-EM) algorithm, an image of the positron emitting source was reconstructed.

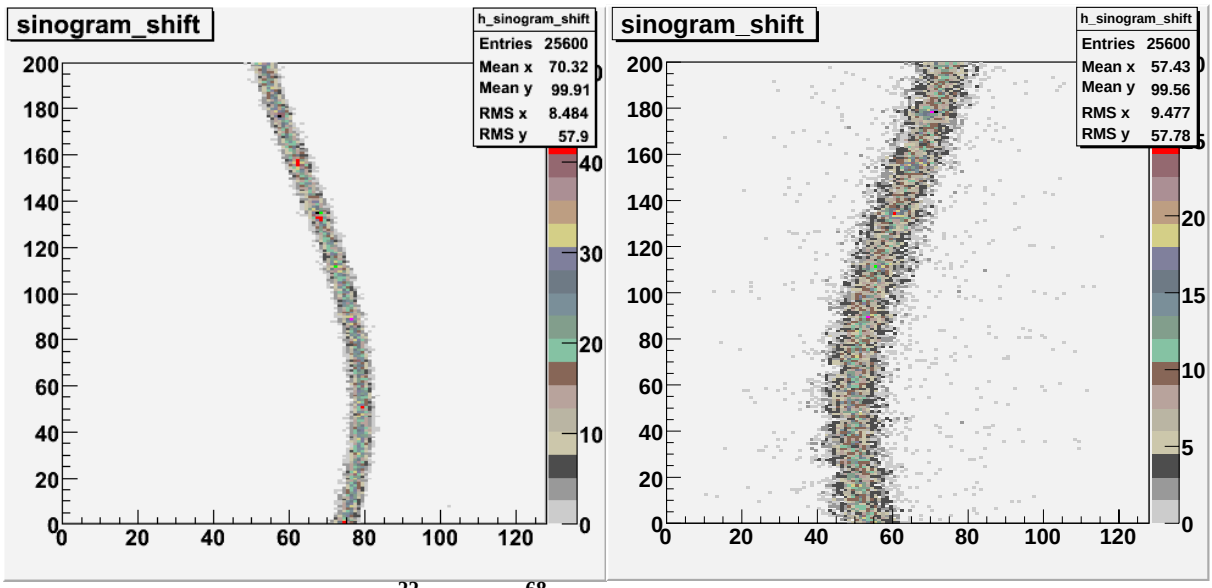

Figure 6: Sinograms for ^{22}Na and ^{68}Ga isotopes.

V. Comparison of Simulation to Reality

With simulations showing that magnetic fields were a feasible means of improving PET scan resolution, performing actual experiments with imaging apparatus would ultimately confirm these predictions. In the absence of strong magnetic fields, the photodetector constructed from non-magnetic components was tested. The experimental data obtained from these trials closely matched the expectations established by simulation, as observed in Figure 7 and Table 1 [13].

	0.25 mm ^{22}Na Source		1.0 mm ^{68}Ga Source	
Simulated Data	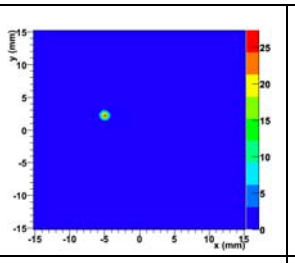	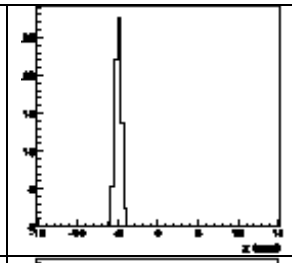	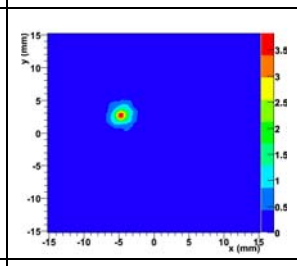	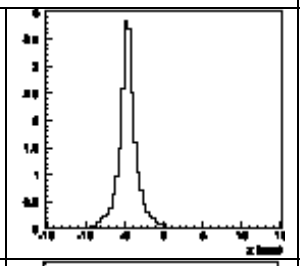
Experimental Data	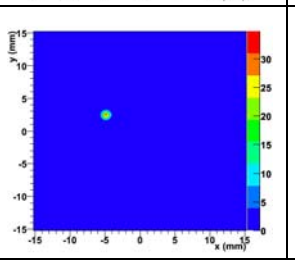	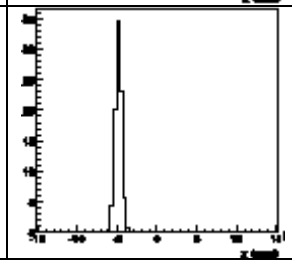	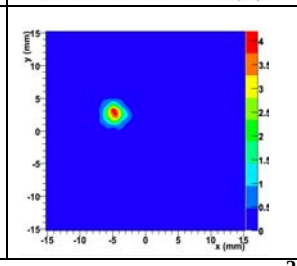	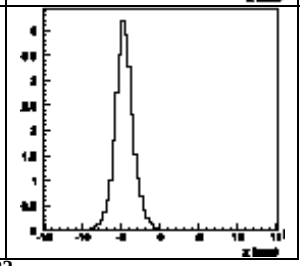

Figure 7: A comparison of simulated data versus experimental results for ^{22}Na (545 keV maximum emitted positron energy) and ^{68}Ga (1899 keV maximum emitted positron energy for this one, too) isotopes in the absence of a magnetic field.

Source	Data Type	X FWHM (mm)	X FWTM (mm)	X RMS (mm)	Y FWHM (mm)	Y FWTM (mm)	Y RMS (mm)
^{22}Na (0.25 mm disk source)	Simulated	0.9	1.6	0.4	0.9	1.7	0.4
	Real	0.9	1.7	0.4	0.9	1.6	0.4
^{68}Ga (1.0 mm disk source)	Simulated	1.6	4.7	1.4	1.6	4.3	1.4
	Real	2.3	4.7	1.4	2.3	4.7	1.3

Table 1: A numerical comparison of image reconstruction properties for real and simulated ^{22}Na and ^{68}Ga trials.

In collaboration with the Ohio State University Medical Center, the detector system was tested in the presence of a 7 Tesla magnetic field at the Wright Center of Innovation in Biomedical Imaging. Again, expectations were confirmed by experimental data, as a test of resolving power of the detection system showed strong agreement with simulation. Two 1.0 mm ^{68}Ga disk sources, one with a tenth of the activity of the other source, were positioned 3.6 mm apart in the imaging plane of the prototype detector. The system performed scans in 0 T and 7 T magnetic field environments. A comparison of projections in the x-direction for experimental and simulation data for both conditions are shown in Figure 8 [14].

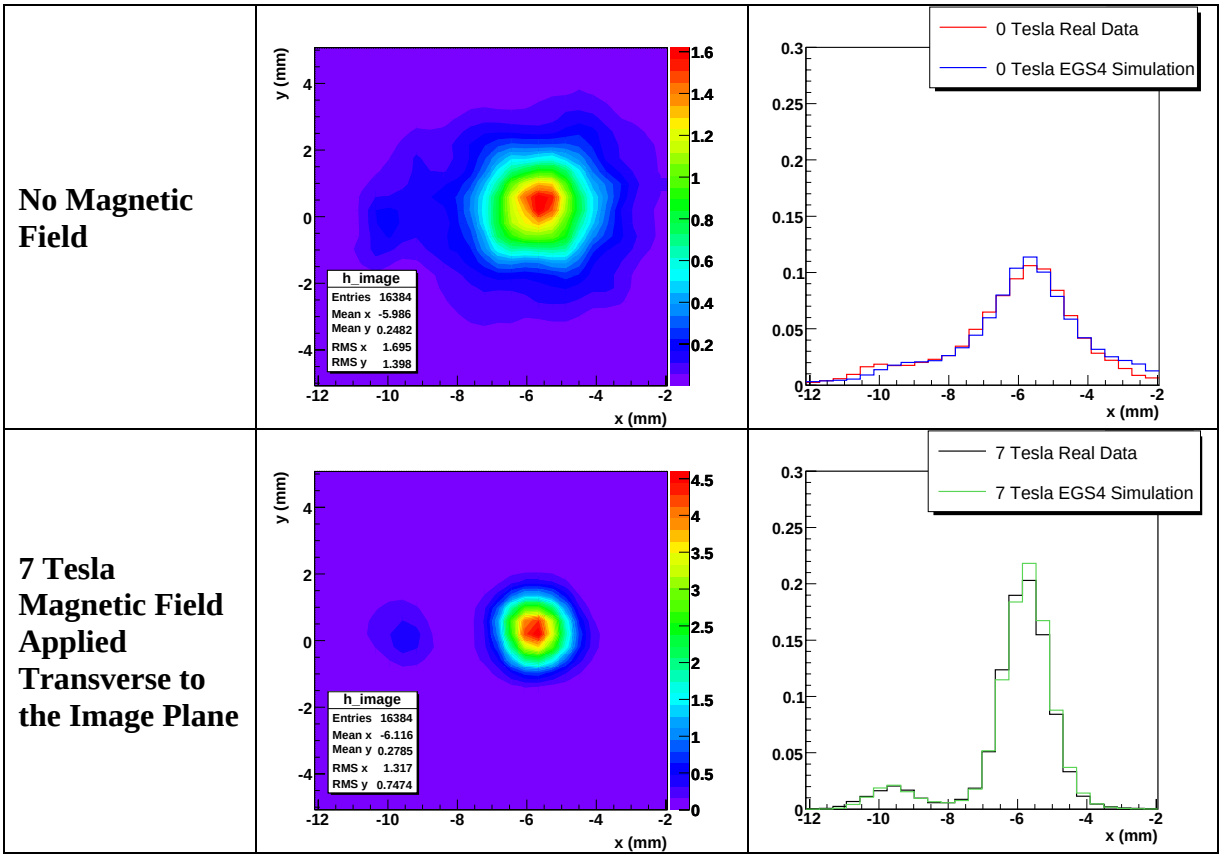

Figure 8: A comparison of simulation to experimental data in a strong magnetic field. Two 1.0 mm ^{68}Ga sources, the right one with ten times the activity, were placed 3.6 mm apart and imaged with and without a 7 Tesla magnetic field. The distributions on the right contain simulation data superimposed over experimental values.

VI. Conclusions

The introduction of static magnetic fields to the particle simulation utility EGS4 showed that the presence of a strong magnetic field could improve the resolution of PET images taken with the novel silicon-silicon pad detector system developed in the laboratory of Dr. Honscheid. In particular, there was a positive relationship between magnetic field strength and resolution improvement (figure 9). This was found to reduce blurriness associated with both the use of high-energy radioactive isotopes and the emission of positrons in electron-sparse media. This was illustrated through simulation of ^{18}F (lower energy, 635 keV maximum positron energy) and ^{94m}Tc (higher energy, 2470 keV maximum positron energy) isotopes in water and lung (~1/3 the density of water). As Figure 10 illustrates, the higher-energy isotopes and lower-density media can be attributed to greater positron displacement from the source prior to annihilation, while the presence of a strong magnetic field – 9 T in this case – effectively confines the positron to a circular path closer to the source in each of these situations.

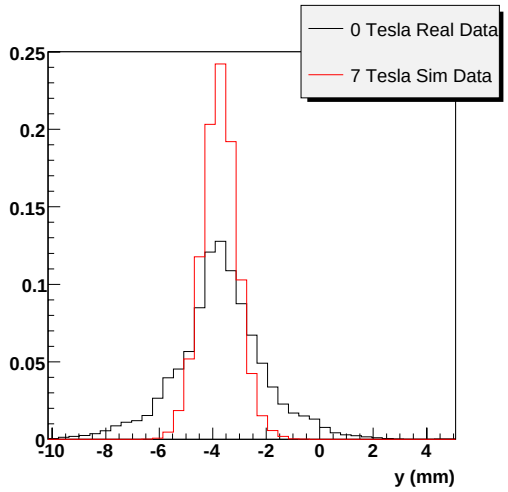

Figure 9: A comparison of image resolution versus magnetic field strength for a ^{68}Ga isotope.

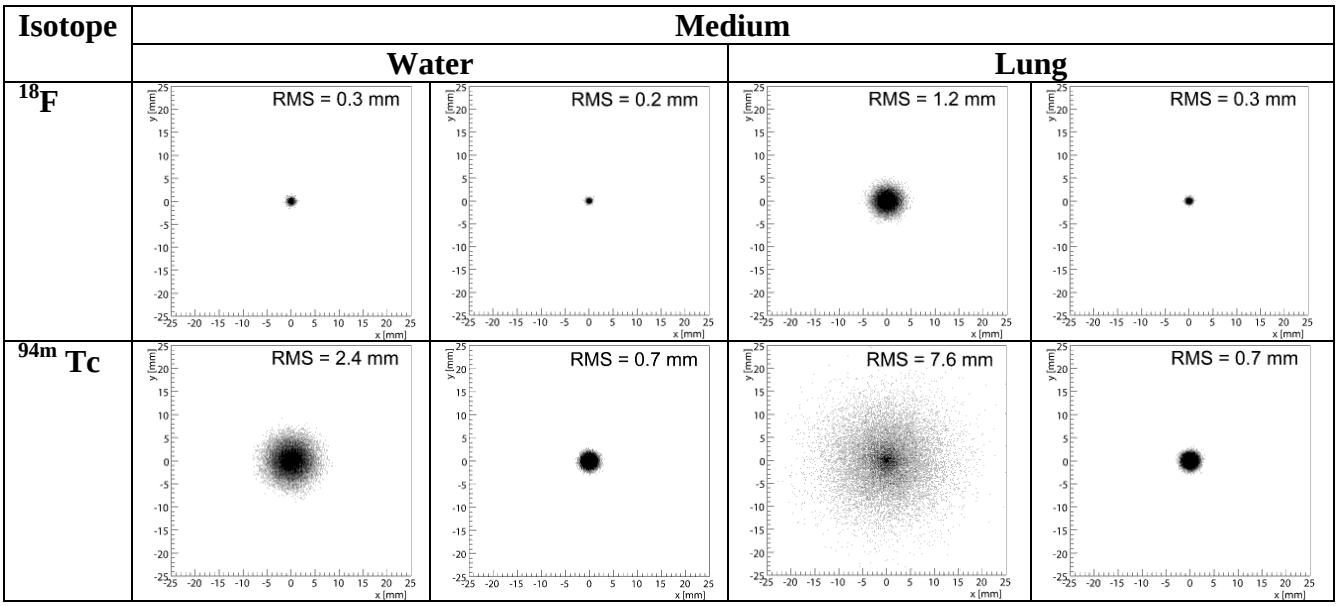

Figure 10: The effects of radioactive isotope energy and media on displacement of positrons from their source prior to annihilation. ^{18}F has a maximum positron energy of 635 keV, while ^{94m} Tc has a maximum positron energy of 2470 keV. Body tissues have a density comparable to water, while lung tissue has about 1/3 the density of water.

The successful testing of a strong magnetic field simulation was met by experimental trials of the prototype scanner. Strong agreement was observed between simulation and experimental data in the absence of a magnetic field. In a collaborative effort with the Ohio State University Medical Center, the experimental apparatus was tested in the presence of a 7 Tesla magnet. Testing the novel detector system in the presence of the strong magnetic field confirmed the expectations established by simulation. Given the successful testing of a silicon-silicon detector system and its improved resolution over existing PET scanners, the additional improvement of resolution associated with strong magnetic fields shall make this a more versatile research and diagnostic utility in the future.

References

[1] G. F. Knoll, *Radiation Detection and Measurement*, Third Edition, Wiley Inc., Hoboken, NJ, USA, 2000.

[2] R. N. Beck, "Imaging Science: Bringing the Invisible to Light," M. N. Wernick, J. N. Aarsvold, *Emission Tomography: The Fundamentals of PET and SPECT*, Elsevier Academic Press, San Diego, USA, (2004) 1.

[3] G. L. Zeng et al., "Single-Photon Emission Computed Tomography," M. N. Wernick, J. N. Aarsvold, *Emission Tomography: The Fundamentals of PET and SPECT*, Elsevier Academic Press, San Diego, USA, (2004) 127.

[4] M. N. Wernick, J. N. Aarsvold, "Introduction to Emission Tomography," M. N. Wernick, J. N. Aarsvold, *Emission Tomography: The Fundamentals of PET and SPECT*, Elsevier Academic Press, San Diego, USA, (2004) 12.

[5] R. Lecomte, "Technology challenges in small animal PET imaging," *Nuclear Instruments and Methods in Physics Research* A 527 (2004) 157.

[6] S. Park et al., "A prototype of very high-resolution small animal PET scanner using silicon pad detectors," *Nuclear Instruments and Methods in Physics Research* A 570 (2007) 543.

[7] T. Lewellen, J. Karp, "PET Systems," M. N. Wernick, J. N. Aarsvold, *Emission Tomography: The Fundamentals of PET and SPECT*, Elsevier Academic Press, San Diego, USA, (2004) 179.

[8] Shibuya, K. et al., "A Healthy Volunteer FGD-PET Study on Annihilation Radiation Non-collinearity," *IEEE Nuclear Science Symposium Conference Record*, (2006) 1889.
[9] P. E. Kinahan, M. Defrise, R. Clackdoyle, "Analytic Image Reconstruction Methods," M. N. Wernick, J. N. Aarsvold, *Emission Tomography: The Fundamentals of PET and SPECT*, Elsevier Academic Press, San Diego, USA, (2004) 421.
[10] R. R. Raylman, B. E. Hammer, N. L. Christensen, "MRI-PET Scanner Design: The Effect of Magnetic Fields on the Intrinsic Resolution of PET Scanners," IEEE TNS 43, (1996) 2406.
[11] W. R. Nelson, H. Hirayama, D. W. O. Rogers, "The EGS4 Code System", *Report SLAC-265*, Stanford Linear Accelerator Center, Stanford, California, 1985.
[12] C. S. Levin and E.J. Hoffman, "Calculation of positron range and its effects on the fundamental limit of positron emission tomography system spatial resolution," *Physics in Medicine and Biology*, (1999) 44: p.781-799.
[13] D. Burdette, et al, "Very High Resolution Small Animal PET Using Solid-State Detectors in a Strong Magnetic Field," *IEEE Nuclear Science Symposium Conference Record*, 2006.
[14] D. Burdette, et al, "A Study of the Effects of Magnetic Fields on the Image Resolution of PET Scanners," *IEEE Nuclear Science Symposium Conference Record*, 2007.